Reliability of velocity measurements made by monopole acoustic logging-while-drilling tools in fast formations

Citation: Wang, Hua et al. "Reliability of Velocity Measurements Made by Monopole Acoustic Logging-While-Drilling Tools in Fast Formations." GEOPHYSICS 82, no. 4 (May 30, 2017): D225–D233 © 2017 Society of Exploration Geophysicists

As Published: http://dx.doi.org/10.1190/GEO2016-0387.1

Publisher: Society of Exploration Geophysicists

Persistent URL: http://hdl.handle.net/1721.1/114235

Version: Final published version: final published article, as it appeared in a journal, conference proceedings, or other formally published context

GEOPHYSICS, VOL. 82, NO. 4 (JULY-AUGUST 2017); P. D225–D233, 8 FIGS., 1 TABLE.
10.1190/GEO2016-0387.1

Reliability of velocity measurements made by monopole acoustic logging-while-drilling tools in fast formations

Hua Wang[1], Michael Fehler[1], and Douglas Miller[1]

ABSTRACT

The accuracy of velocity measurements made using a monopole acoustic logging-while-drilling (ALWD) measurement tool is influenced by the eccentering of the tool due to complex drill string movements. We have used the velocity of collar flexural mode (at the source frequency range) as a reference and classified the fast formations into (1) fast-fast (FF) formations with compressional velocity far larger than the collar flexural velocity and (2) slow-fast (SF) formations with compressional velocity approaching that of the collar flexural velocity. We use a 3D finite-difference method to simulate the response of an eccentered monopole ALWD tool with different eccentering magnitudes (offsets) for the two types of formations to facilitate better interpretation of velocity measurements made in an actual drilling environment. We find that the collar extensional mode, existing in the centralized and eccentered tool cases, only affects the formation P-wave measurement and can be eliminated by using an isolator. The collar flexural mode, which is a shear motion in the collar and can only be excited in a centralized tool by a dipole source, is also excited when a monopole tool is eccentered, and it significantly affects the measurement of the compressional velocity in the SF formation and that of the shear velocity in the FF formation, even for small eccentering offsets. Thus, the uncorrected monopole ALWD tool provides unreliable formation velocities (either the compressional or shear velocities) in fast formations because of the significant influence of the tool offsets on the measurement. To minimize the influence of tool offset on the measurements, we compared the differences between the waveforms collected for different azimuths and tool offsets and the centralized monopole waveforms.

INTRODUCTION

In the acoustic logging community, we classify formations into fast and slow according to the relationship between the formation shear velocity and the borehole fluid compressional velocity. If the formation shear velocity is larger than the fluid compressional velocity, the formation is designated as a fast formation. Otherwise, the formation is referred to as a slow formation. Different measurement tools have been developed for formation velocity measurements in each type of formation.

As an advanced technology, acoustic logging-while-drilling (ALWD) is commonly used to determine the elastic parameters of a formation during drilling (Wang et al., 2009a). A large number of studies on ALWD have shown that the velocities of the P-wave and S-wave can be reliably measured in fast formations by a monopole tool accompanied by the effect of the collar extensional mode on the P-wave being eliminated by some means (Leggett et al., 2001; Wang et al., 2009b; Kinoshita et al., 2010; Su et al., 2015).

An idealized logging tool is a rigid cylinder centered within a cylindrical borehole. In practice, even when mechanical centralizers are used, the central axis of the tool may not perfectly coincide with the central axis of the borehole. In the simplest case, the two axes are parallel, but the tool axis is offset from the borehole axis. In this case, the tool is eccentered with respect to the borehole and a single eccentering vector defines the azimuth and magnitude of the eccentering (offset). In general, the tool might be tilted and eccentered with respect to the borehole, requiring a description in terms of a pair of eccentering vectors or some equivalent method.

The complex movements and the weight of the drill pipe lead to the tool being off-center in ALWD field applications, which will inevitably affect the measurement of formation velocities. Previous studies of eccentered ALWD tools have mainly focused on the

Manuscript received by the Editor 21 July 2016; revised manuscript received 15 March 2017; published online 30 May 2017.
[1]Massachusetts Institute of Technology, Earth Resources Laboratory, Cambridge, Massachusetts, USA. E-mail: wanghua@mit.edu; fehler@mit.edu; demiller@mit.edu.

responses of dipole and quadrupole LWD tools (Huang 2003; Tang et al., 2009). Huang (2003) and Wang et al. (2013a, 2015) have studied the response of an off-center monopole tool. Pardo et al. (2013) use a finite-element method to study the responses of eccentered monopole tools in the fast and slow formations for a few ALWD scenarios.

In our previous study (Wang et al., 2015), we investigate the response of an eccentered monopole tool in a fast formation. However, the effect of the tool eccentering on velocity measurement has not yet been quantified. Here, we characterize fast formations by their P-wave velocities relative to the collar flexural wave velocity and use finite-difference simulation to study the wavefield recorded by an eccentered monopole tool in two fast formation categories. A high-resolution velocity-time semblance method (Kimball and Marzetta, 1986) is used for determining the formation velocities from the calculated array waveforms as tool offset varies. Using our binary classification of formations, we analyze the velocity measurements in different fast formations.

METHOD AND MODEL

To simulate a large borehole sonic logging model with limited computer memory and computation time, a stretched grid is usually used. In the stretched grid finite-difference method, the fine grids are adopted near the borehole, and the coarse grids are used far away from the borehole. The thin grids allow us to reliably describe the geometry of the circular borehole (Huang, 2003; Tao et al., 2008). However, some problems can appear with improper treatment of the stretched grid, such as unphysical reflections at the interface between the coarse and fine meshes, and numerical instability (Kristek et al., 2010). These issues can be controlled with very careful treatment (Kristek et al., 2010). To simplify the treatment of the stretched grid for borehole sonic logging simulation while retaining increased efficiency, we chose to keep a uniform fine grid (1 mm grid size) in the x-y-planes (normal to the borehole axis) while using a coarse grid (3 mm grid size) in the z-direction (parallel to the borehole axis). The fine mesh in the horizontal plane allows us to describe the borehole geometry, and the coarse mesh along the borehole axis direction is used to simulate the full length of the sonic tool. Our finite-difference code has second-order accuracy in space and time.

Figure 1a and 1b shows the top-down and side views of the borehole model, respectively. Media properties and geometries are given in Table 1. The acoustic sources are embedded on the outer edge of the drill collar. Thirty-six point sources are used to simulate the response of the ring source. Sources having identical phases are simultaneously energized at all 36 point sources for the monopole tool simulation. A total of 36 point receivers are also located around the collar for each receiver interval (8 receiver stations in total). The receiver azimuth is measured relative to receiver 1, where receiver 1 has azimuth angle of 0°, receiver 10 at 90°, receiver 19 at 180°, and receiver 28 at 270°. The dimensions of the simulation model are 0.6, 0.6, and 4.55 m in x, y, and z, respectively. The borehole center is (0, 0) in the x-y-plane in Figure 1a, which means that the coordinates for receivers 1, 10, 19, and 28 are (0.09, 0), (0, 0.09), (−0.09, 0), and (0, −0.09), respectively. The source is located at $z = 0$ m, and the receivers at eight different offsets are located from $z = 3$ m to $z = 4.05$ m with a minimum source-receiver spacing of 3 m and receiver offset separation of 0.15 m along the borehole. The complex frequency-shifted perfectly matched layer method (with the absorbing layers of 20 grids on each side of the 3D model) is used to eliminate the reflection from the truncated boundary of the simulation region (Wang et al., 2013b). In the following discussion, we shift the entire tool to an equal amount moving receiver 1 toward the edge of the borehole (positive direction of x-axis). Our source function is a 10 kHz Ricker wavelet.

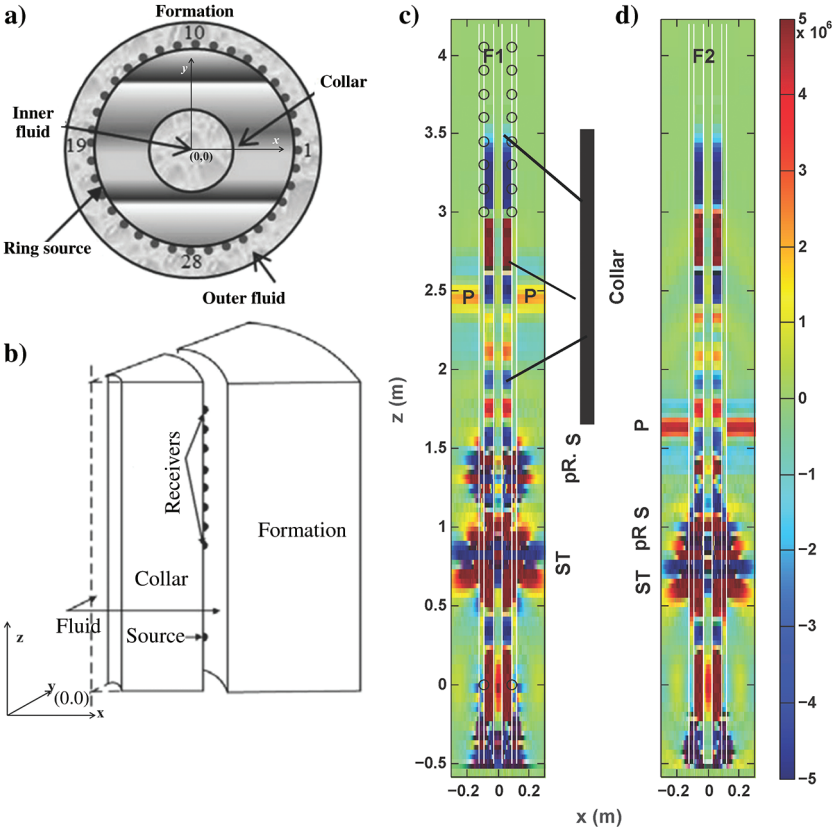

Figure 1. Model used for the ALWD simulation and pressure snapshots: (a) top-down view, (b) side view, pressure snapshots at 0.7 ms for the x-z profile for a centralized tool for fast formations (c) F1 and (d) F2. The source and receivers are marked by circles in (c). There are six solid white lines from $z = -0.45$ m to $z = 4.1$ m. The two innermost lines around $x = 0$ are the boundaries for the inner fluid, the two outermost lines are boundaries of the borehole wall, and the other two lines are the outer boundary of the collar.

tended to facilitate a detailed investigation of the monopole tool eccentering on P-wave and collar wave, and F1 was selected to study the S-wave and collar wave. In general, when the velocity gap between the collar and formation is small as in F1, it is hard for data collected by a monopole AWLD tool to distinguish the P-wave from the collar extensional wave, except with the use of an isolator (Kinoshita et al., 2010; Su et al., 2015).

NUMERICAL RESULTS

ALWD wavefield in fast formations

Part of the ALWD wavefield propagates along the collar and has a strong influence on the formation wave measurements. Different collar waves are excited with different ALWD tools according to the characteristics of the collar wave in different cases (Wang et al., 2016). The collar extensional wave, which is excited when the monopole tool is used, has a weak dispersion with the velocity being 0.8–0.9 times the compressional velocity of the collar (see Figure 2c in Wang et al., 2016). The collar flexural wave is a shear motion of the collar that is excited by a dipole source. The collar flexural wave has a strong dispersive behavior with velocity from 0 m/s at 0 Hz to approximately 0.8 times the shear velocity of the collar material at high frequency (more than 10 kHz) (see Figure 12 in Wang et al., 2016).

Example wavefields in centralized monopole ALWD tool models are shown in Figure 1c and 1d, which shows snapshots of the x-z profiles of pressure at 0.7 ms (from the excitation time of the wavelet [first motion time of the wavelet: 1.5/{source frequency}, 0.15 ms for 10 kHz]) for centralized monopole tools in formations F1 and F2, respectively. The snapshots show the entire computation region (e.g., the region in the z-direction is from −0.45 to 4.1 m), including the absorbing layer. There are six solid white lines from $z = -0.45$ m to $z = 4.1$ m. The two innermost lines around $x = 0$ are the boundaries for the inner fluid, and the two outermost lines are the boundaries of the borehole wall. The other two lines are the outer boundary of the collar. The positions of the sources and receivers are marked by circles in Figure 1c. The pressure snapshots show the collar extensional mode with the same color in the right and left sides of the collar. The black bar marks in Figure 1c indicate the propagation spatial range of this mode. The formation P-wave can also be found in the snapshots. However, it cannot be clearly identified in the borehole in formation F1 (Figure 1c) because it is within the collar extensional wave packet, which is usually eliminated by the use of isolators on commercial logging tools. Formation S-wave and pR (pseudo-Rayleigh)-wave around $z = 1.5$ m are the shear motion around the borehole. The Stoneley waves, the slowest borehole guided waves, can be found in the snapshots and are marked around $z = 0.8$ m in Figure 1c. These waves penetrate deeply into the formation due to their low frequency. More details on the various modes in the borehole can be found in Haldorsen et al. (2006).

The wavefront of the modes identified in Figure 1c can also be found in Figure 1d. However, the P-wave in Figure 1d is separated from the collar extensional wave in the borehole because of the large velocity gap between the collar extensional and P-wave. This suggests a possible approach for eliminating the interference of the collar extensional wave on the P-wave velocity measurement when using monopole tools in fast formations: using a collar made of a material with large velocity rather than adding an isolator on the collar (Wang et al., 2016). Our choice of formation F2 was made to allow us to investigate the effects of tool eccentering on P-wave measurements when an isolator is not present in the ALWD tool.

We show pressure snapshots of the wavefield at 0.7 ms for an eccentered monopole ALWD tool in formations F1 and F2 in

Table 1. Parameters for the borehole models. The V_P and V_S are the formation of P-wave and S-wave velocities, respectively. OR, outer radius; IF, inner fluid; OF, outer fluid; F1 and F2 are the two fast formations.

	V_P (m/s)	V_S (m/s)	Density (g/cm^3)	OR (mm)
IF	1470	—	1.00	27
Collar	5860	3300	7.85	90
OF	1470	—	1.00	117
F1	4500	2650	2.40	—
F2	3000	1800	2.00	—

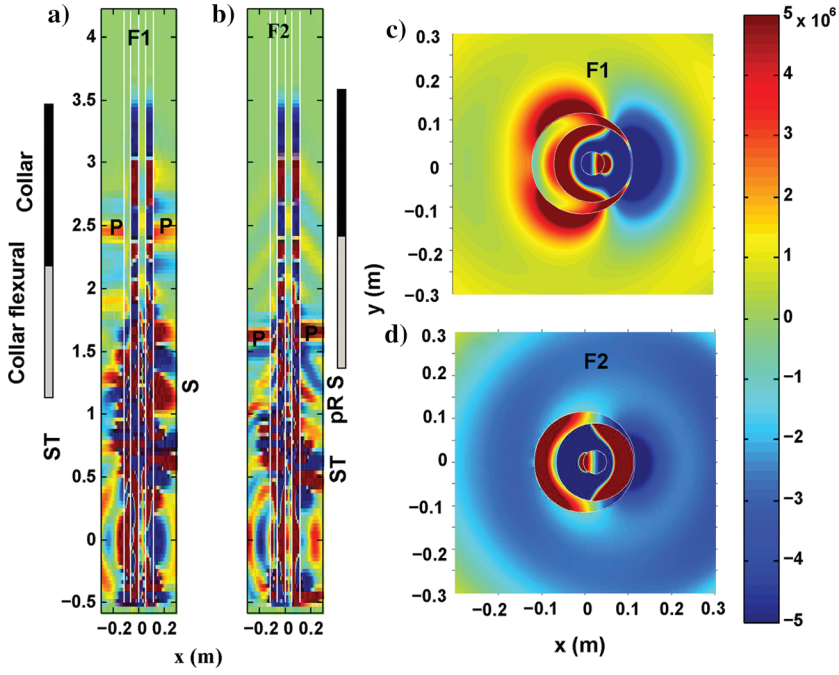

Figure 2. Pressure snapshots at 0.7 ms for different profiles when the eccentering vector is 24 mm long in formations F1 and F2. (a and b) The x-z profiles and (c and d) x-y profiles at $z = 1.53$ m. The two small white circles in (c and d) denote the inner and outer boundaries of the collar, and the largest white circle is the boundary of the borehole. The color bar indicates the relative amplitudes.

Figure 2. The drill collar in both formations is shifted 24 mm toward the x-direction (the smallest fluid column between collar [receiver 1] and borehole wall is 3 mm, whereas the largest fluid column [receiver 19] is 51 mm). The collar flexural mode marked by a gray bar is visible at a distance of 1–2 m (Figure 2a) and 1.5–2 m (Figure 2b) from the source in the x-z snapshot of the pressure. The wavefront of the P-wave on the right side of Figure 2b is advanced relative to that on the left side. The S-wave and pR-waves are no longer distinguishable in the wavefield snapshot in Figure 2a due to contamination by the collar flexural mode. Conversely, the P-wave in the F1 model (Figure 2a) and S-wave in the F2 (Figure 2b) model are little influenced by tool eccentering.

The pressure snapshots for the top-down view x-y profile at 1.53 m along the borehole axis relative to the source position are shown in Figure 2c (F1) and 2d (F2). The two small white circles in the figure sections denote the inner and outer boundaries of the collar, and the largest white circle is the boundary of the borehole. The azimuthal variation of color appearing in the collar snapshots at different positions corresponds to the flexural mode (the color bar is given in the figure sections). The colors showing the wavefield in the collar are the same at azimuths of 90° and 270°.

Our results show that the appearance of the collar flexural wave interferes with the P-wave in formation F2 and the S-wave in formation F1 when the monopole tool is eccentered. We propose that fast formations in ALWD can be classified into two types according to a critical velocity, the velocity of collar flexural wave at the source frequency range: (1) fast-fast (FF) formations with P-velocity far larger than collar flexural velocity and (2) slow-fast (SF) formations with P-wave velocity approaching the collar flexural velocity. This classification is similar to the method used to classify cement according to the velocity of the flexural mode in the casing (van Kuijk et al., 2005).

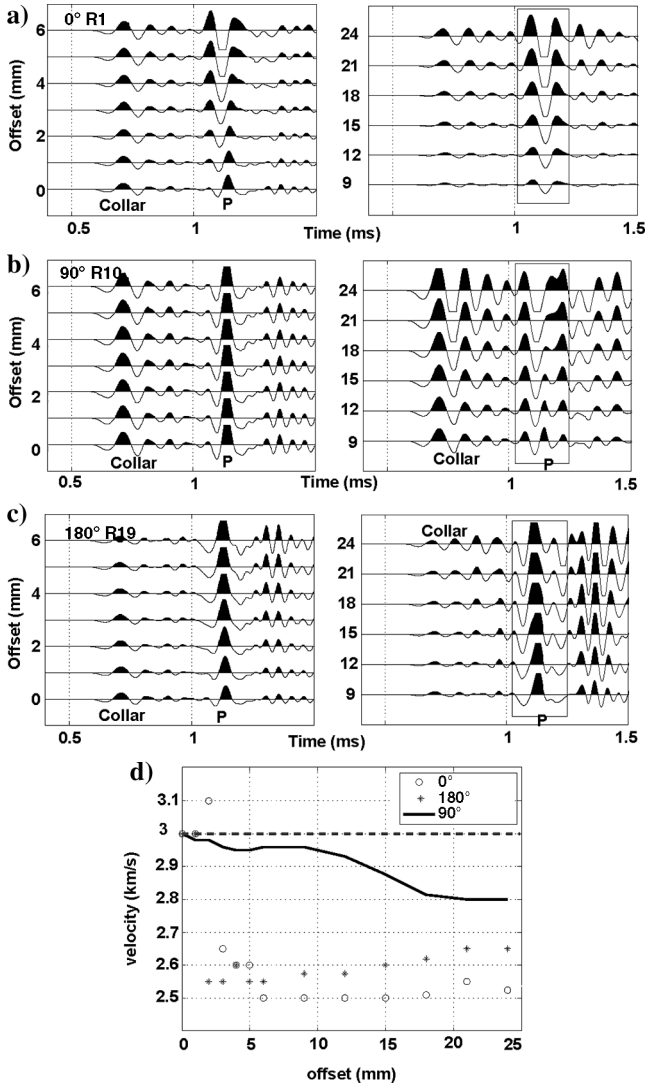

Figure 3. Waveforms at receivers for three azimuth angles in formation F2 for different tool offsets: (a) 0° azimuth angle; (b) 90° azimuth angle; (c) 180° azimuth angle; (d) P-wave velocity obtained from waveforms at 0°, 90°, and 180° azimuth angles (the dashed blue line is the correct value of the shear velocity). Trace amplitudes are normalized by the maximum one in each plot, in which the maximum amplitudes for waveforms with offsets from 0 to 6 mm and from 9 to 24 mm are chosen separately.

The influence of monopole ALWD tool eccentering on P-wave velocity measurement in the fast formation F2

Here, we focus on P-wave velocity measurement in an SF formation (F2) with different tool offsets. We evaluate the waveforms at receivers having four different azimuthal angles at an axial position located 3 m from the source. Figure 3 shows the waveforms at different receivers (different azimuth angles) as the tool offset changes from 0 to 24 mm.

Figure 3a shows the waveforms at receiver 1 with azimuth angle of 0°. Trace amplitudes are normalized by the maximum one in each plot, in which the maximum amplitudes for waveforms with offsets from 0 to 6 mm and from 9 to 24 mm are chosen separately. We can see that the arrival time and shape of the collar (extensional) wave, labeled on the left panel of Figure 3a, do not change, whereas the amplitude becomes larger with the increase of eccentering. The wave following the collar wave, which is supposed to be a P-wave, becomes dispersive and has a higher amplitude with the increasing tool offset at this receiver. Considering the snapshot in Figure 2b and the waveforms in Figure 3, we believe that the P-wave is submerged in the latter portion of the dispersive collar flexural wave at the receiver located in the direction of the tool offset.

Figure 3b shows the waveforms at receiver 10 (azimuth angle of 90°) with various tool offsets. When the tool offset is less than or equal to 6 mm, we find that the observed modes are nearly the same as those in the centralized tool case. For large tool offsets (larger than 9 mm), we find that the wave amplitude increases with increasing tool offset and it is difficult to identify the P-wave.

We use a velocity-time semblance method (Kimball and Marzetta, 1986) to calculate the P-wave velocity from array waveforms at receiv-

ers with different azimuth angles when tool offsets range from 0 to 24 mm. Figure 3d shows the P-wave velocities obtained for different tool offsets using waveforms at receivers with azimuth angle of 0°, 90°, and 180°. Except for the smallest eccentering (1–3 mm), the estimated P-wave velocity from the waveforms using receivers at 0° and 180° is significantly below the velocity of collar flexural wave around the source frequency (at approximately 2800 m/s at 10 kHz) and the formation P-wave velocity of 3000 m/s. This could cause misinterpretation of field measurements because it is hard to limit the offset to less than 3 mm. For the waveforms at a 90° azimuth angle, the errors in the P-wave velocity determination are much smaller, with a mismatch of less than 3%, for eccentering 10 mm or less.

We conclude that for the waveforms at receivers with azimuth angles of 0° and 180° in an SF formation such as F2, the P-wave is affected by the induced collar flexural wave when the monopole tool is eccentered, whereas the S-wave is not affected. Although the use of an isolator on commercial tools eliminates almost all the influence of the collar extensional wave on the P-wave, the collar flexural wave that is present when the tool is off center cannot be eliminated because the isolator is only designed to eliminate the collar extensional wave. The P-wave velocity will thus be incorrectly determined by ALWD in this fast formation, which agrees with conclusions in our previous study (Wang et al., 2015).

The influence of monopole ALWD tool eccentering on S-wave velocity measurement in the fast formation F1

We now focus on the S-wave velocity measurement in an FF formation (F1) with different tool offsets. We evaluate the waveforms at receivers having three different azimuthal angles at an axial position located at 3 m from the source. Figure 4 shows the waveforms at various azimuths when the tool offset varies from 0 to 24 mm. The waveforms between 1.1 and 1.5 ms contain the S-wave and pR-wave when the tool is centralized. The tool eccentering makes these modes dispersive and they lose coherence. For waveforms at an azimuth angle of 0° (Figure 4a), we find that the arrival time of the S-wave is hard to detect when the tool offset is greater than 2 mm because of the overlap between the collar wave and S-wave. Figure 4b shows the waveforms (1.1–1.8 ms) at receiver 10 for various eccentering magnitudes corresponding to the window containing S-waves and pR-waves. Larger amplitude coda waves appear in the latter part of the traces (after 1.5 ms) when the tool offset is greater than 9 mm. The S-wave velocity can be determined when the tool offset is less than 6 mm. However, it becomes difficult to determine when the offset exceeds 6 mm. It is similarly easy to detect the S-onset for the waveforms at receiver 19 (at the azimuth angle of 180°) when the tool offset is below approximately 6 mm. For larger offsets, the flexural collar overwhelms the S-wave, as shown in the right panel of Figure 4c.

Figure 5 shows velocity-time semblance plots for the portions of the waveforms between 1.1 and 1.9 ms at different tool offsets for different receiver azimuths (0°, 90°, and 180°). The coherence of the array waveforms at azimuth 0° (Figure 5a) decreases when the tool offset exceeds 2 mm, and there are additional coherent areas ahead of or behind the traveltime of the S-wave due to the dispersive collar flexural wave that makes the shear velocity hard to measure.

For the waveforms at 90° azimuth receivers (Figure 5b), we find that the S-wave velocity can be picked from the maximum value of semblance when the tool offset is 5 mm or less. However, it becomes difficult to pick when the tool offset exceeds 5 mm due to interference by the high-coherence areas before 1.2 ms. The new coherence (before 1.2 ms) will likely be misjudged as S-wave-related information. We see from Figure 5c (azimuth angle of 180°) that the S-wave velocity cannot be obtained even for a very small tool eccentering (1 mm). Similar to Figure 3c, we also plot the velocities picked from the semblance for different tool offsets for waveforms on receivers at three azimuths (as shown in Figure 6, dashed blue line denotes the formation shear velocity). It is very hard to pick the velocity from the semblance because there are

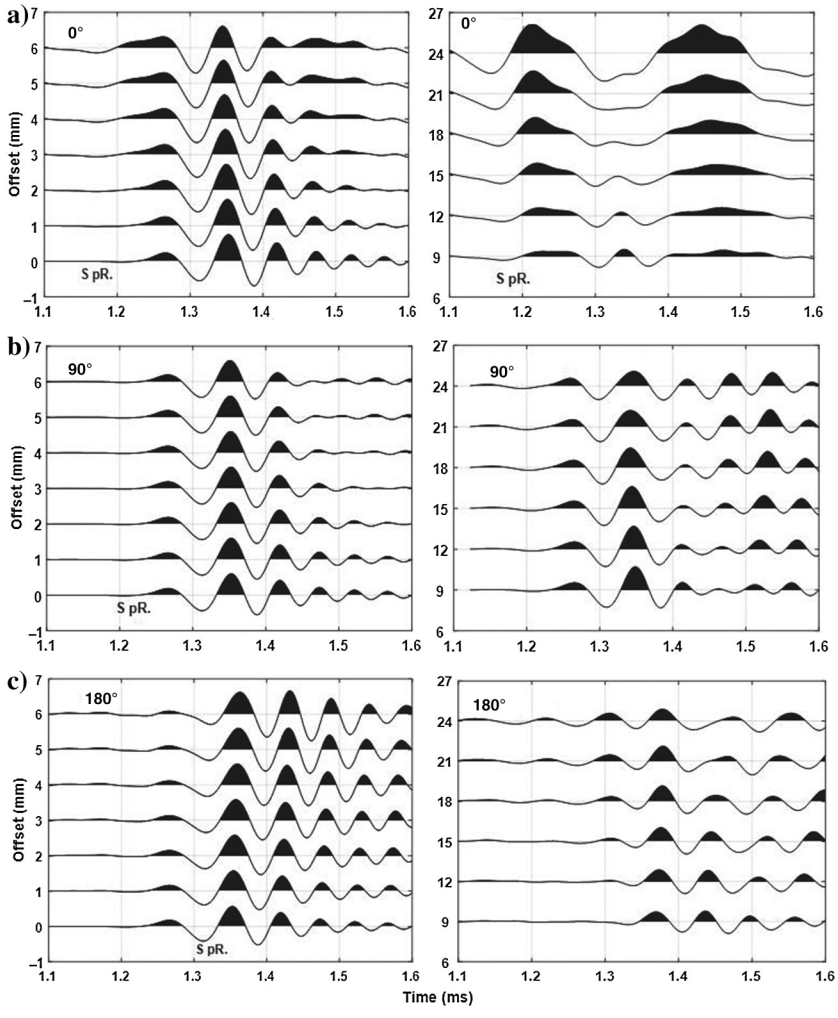

Figure 4. Waveforms at (a) receiver 1, (b) receiver 10, and (c) receivers 19 in formation F1 with different tool offsets.

several areas with good coherence due to the interference of the dispersive collar flexural wave, and we pick only the value with the maximum semblance.

We conclude that the S-wave is interfered with by a dispersive collar flexural wave and that an S-wave velocity measurement cannot be reliably obtained even for very small tool eccentering magnitude for FF formations.

DISCUSSION

In field applications using a monopole ALWD tool in fast formations, the effect of the collar extensional mode on the formation wave measurements can be eliminated by a sonic isolator when the tool is centralized. However, the collar flexural wave, introduced when the tool is eccentered, significantly affects the formation wave measurements for either P- or S-waves depending on the velocity relationship between the formation and collar flexural waves.

Based on our analysis of pressure snapshots and velocity-time semblance plots, we propose that fast formations can be classified into two types according to a critical velocity, the collar flexural

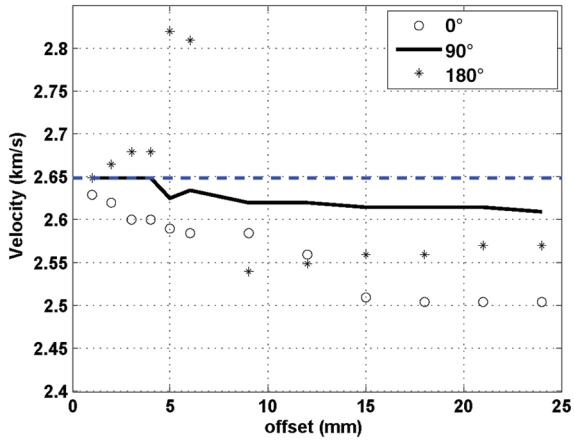

Figure 6. The S-wave velocity obtained from waveforms at 0°, 90°, and 180° azimuth angles. Velocities were chosen at the location of maximum semblance in velocity-time semblance plots such as those in Figure 5. The dashed blue line is the correct value of the shear velocity.

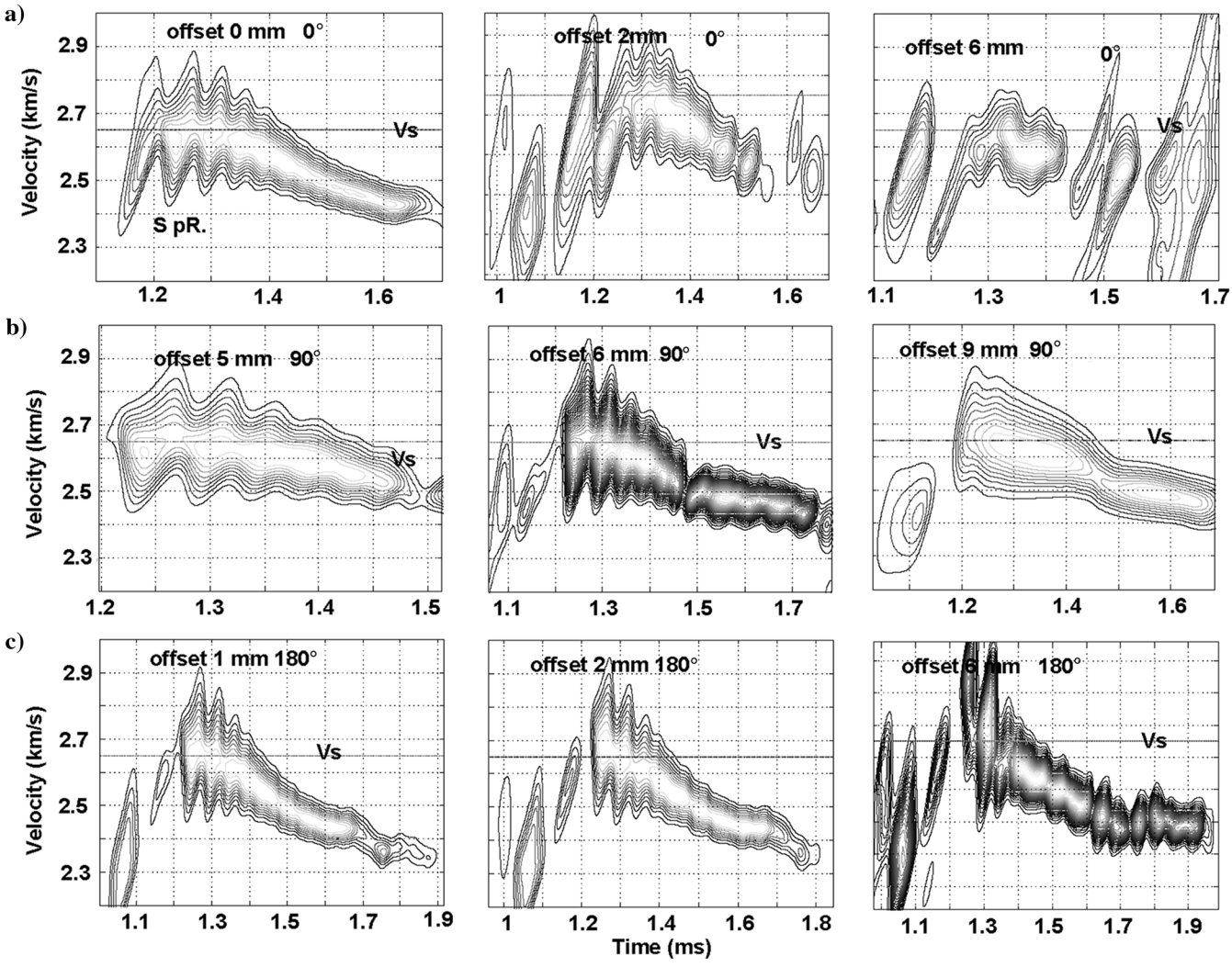

Figure 5. Velocity-time semblance for the S-wave velocity at array receivers with different azimuth angles for different tool offsets in formation F1.

velocity at the source frequency range: (1) FF formations with P-wave velocity far larger than collar flexural velocity and (2) SF formations with P-wave velocity approaching to collar flexural velocity.

For an FF formation, the induced collar flexural wave appears later than the P-wave, and its effects on P-wave determination are small. However, in this case, the collar flexural wave contaminates the S-wave, making S-wave velocity measurement difficult. From analysis of waveforms and velocity-time semblance plots for different tool offset cases, we find that the S-wave is interfered with by the dispersive collar flexural wave and the S-wave velocity determination made from raw waveforms will contain errors for very small tool eccentering magnitudes.

For an eccentered tool in an SF formation, the dispersive collar flexural wave appears ahead of the P-wave, and its long duration leads to it contaminating the P-wave. The P-waves at the receivers suffer different influences depending on their azimuth relative to the tool offset. Even for a very small magnitude of tool offset, the influence of the eccentered tool on the P-wave velocity determination cannot be ignored at some azimuths. Data processing methods based on the presumed asymmetry, such as simple addition of all waveforms from an azimuthal distribution of receivers, will not generally result in a clean P-wave.

In field measurements, a wear band on the tool eliminates large tool offsets. However, small-magnitude tool offsets are likely due to complex movement of the drill pipe. This will inevitably affect the formation velocity measurement.

If the waveforms at receivers of all azimuth angles can be acquired separately, we can possibly identify identical waveforms at the two receivers having an azimuth angle difference of 180°. These receiver positions correspond to the direction orthogonal to the tool offset. Knowing the direction of offset will allow us to determine the receiver in the direction with the smallest fluid column (0°) so that we can avoid using the velocities estimated from receivers at that azimuth. However, the determination of the direction of tool offset is imprecise because of the limited number of receivers (usually four or eight) along the circumference the tool. Although we can quantitatively get the tool offset direction and magnitude based on waveforms from a dipole tool (Wang et al., 2013a), the limited number of receivers means

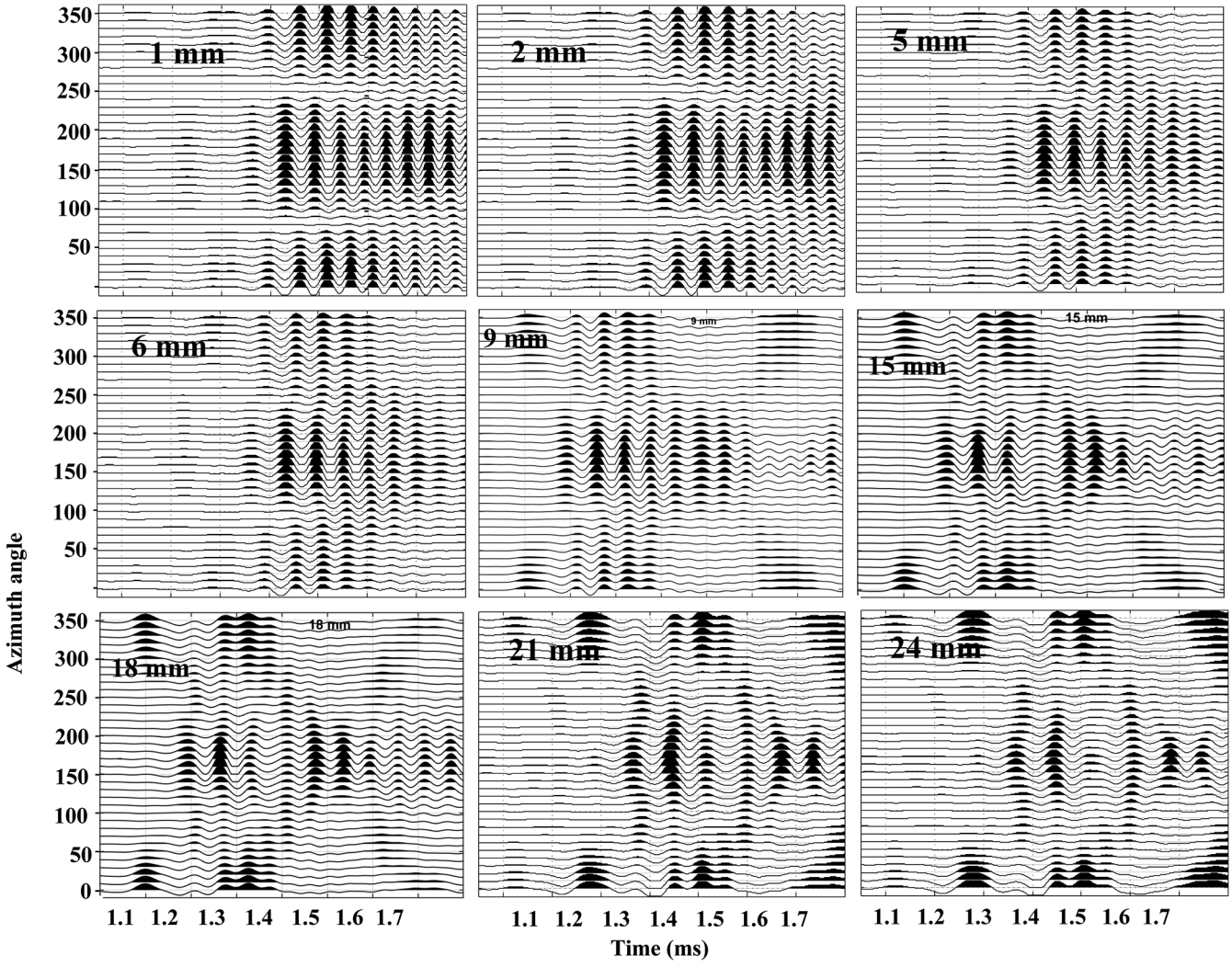

Figure 7. The difference between waveforms for a centralized monopole tool and those for different tool offsets and azimuth angles cases. The tool offsets are listed on the top of each plot. Formation is F1.

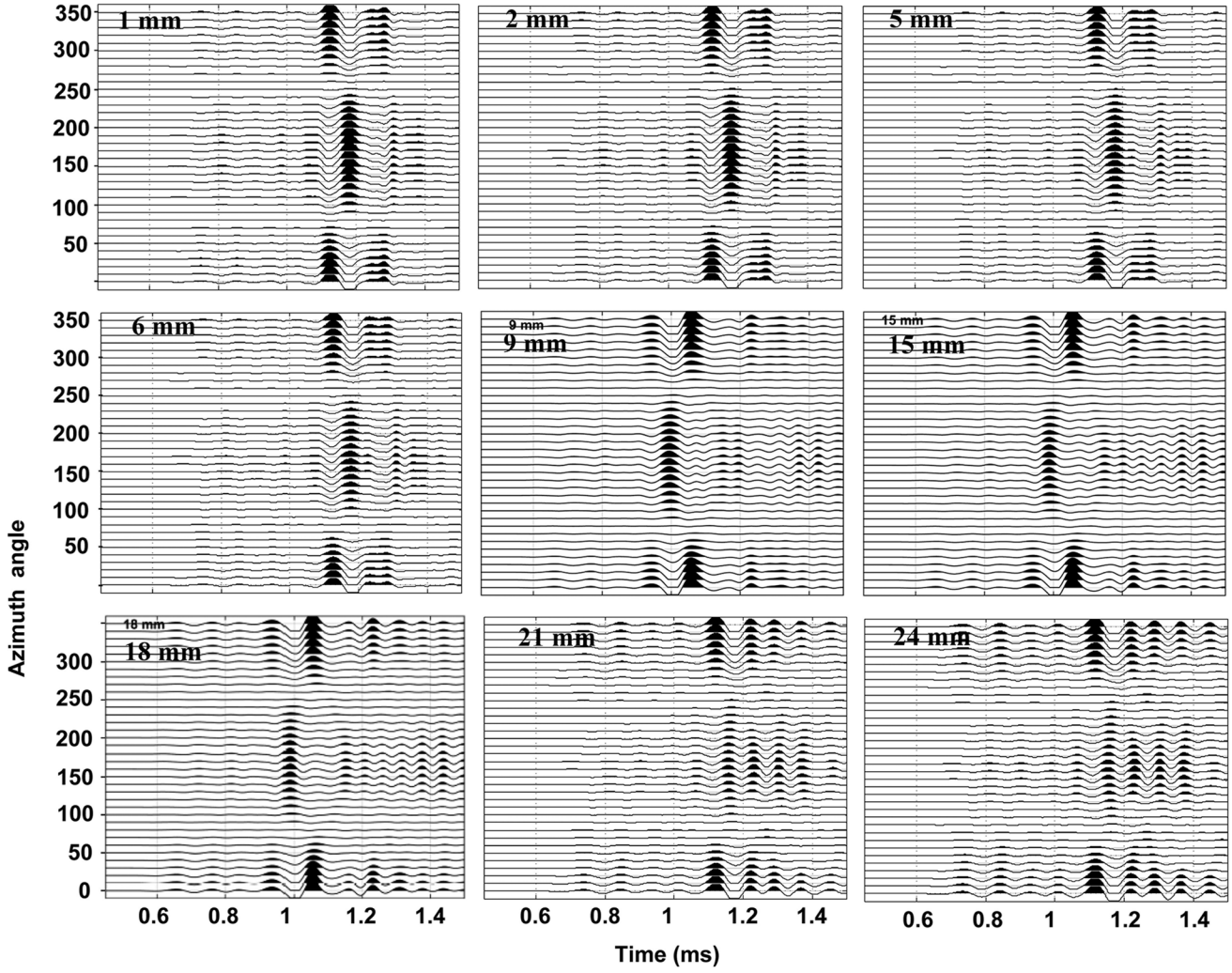

Figure 8. The difference between waveforms for a centralized case and those for different tool offsets and azimuth angles cases. The tool offsets are listed on the top of each plot. Formation is F2.

waveforms at receivers in the tool offset and the orthogonal directions are unlikely to be acquired. Although it is beyond the scope of this paper to make a detailed analysis of possible remedies to improve velocity determination, we believe that the problem might be addressed by quantifying the effects of tool offsets on receivers at different azimuths and then summing those using different weights to synthesize a monopole wavefield. We leave that possibility, together with the problem of how to determine suitable weights, as a suggestion for further work. Figure 7 shows the differences between the waveforms collected for different azimuths and tool offsets and the centralized monopole waveforms in a FF formation, and Figure 8 shows the differences for an SF formation (the source-receiver spacing is 3 m). It is clear from Figure 7 that the differences are nearly zero at 90° and 270° when offsets are less than approximately 6 mm. When the offset increases, the differences have a more complicated pattern. Better quantification of these differences may allow us to develop an inversion technique to recover the monopole waveform from which velocities can be reliably determined. This points toward a future direction for ALWD data processing and tool design.

CONCLUSION

1. We propose that fast formations can be classified into two types according to a critical velocity, the collar flexural velocity: FF formations with P-wave velocity far larger than collar flexural velocity and SF formations with P-wave velocity approaching the collar flexural velocity.
2. For an FF formation, the collar flexural wave will inevitably contaminate the S-wave making the S measurement difficult.
3. For an SF formation, the P-waves at receivers suffer different influences depending on their azimuth relative to the tool offset. In field measurements in which small-magnitude tool offsets cannot be avoided due to complex movement of the drill pipe, this will inevitably affect the formation P-wave velocity measurement.
4. As an approach to remedy the problem that we have documented, we suggest that it might be possible to decompose the waveforms measured in the eccentered case as a sum of the centralized multipole waveforms and to obtain accurate P-wave and S-wave velocities from that decomposition.

ACKNOWLEDGMENTS

This study is supported by a NSFC (no. 41404100) and the Founding Members Consortium of the Earth Resources Laboratory at MIT. H. Wang was partially supported by the International Postdoctoral Exchange Fellowship Program. Our thanks go to X. Wu at ExxonMobil Upstream Research Company for the helpful discussions. The three anonymous reviewers are greatly appreciated for their critical and constructive comments to this work.

REFERENCES

Haldorsen, J. B. U., D. L. Johnson, T. Plona, B. Sinha, H. Valero, and K. Winkler, 2006, Borehole acoustic waves: Oilfield Review (Spring), **18**, 34–43.

Huang, X., 2003, Effects of tool positions on borehole acoustic measurements: A stretched grid finite difference approach: Ph.D. thesis, MIT.

Kimball, C., and T. Marzetta, 1986, Semblance processing of borehole acoustic array data: Geophysics, **49**, 274–281, doi: 10.1190/1.1441659.

Kinoshita, T., A. Dumont, H. Hori, N. Sakiyama, J. Morley, and F. Garcia-Osuna, 2010, LWD sonic tool design for high-quality logs: 80th Annual International Meeting, SEG, Expanded Abstracts, 513–517.

Kristek, J., P. Moczo, and M. Galis, 2010, Stable discontinuous staggered grid in the finite-difference modelling of seismic motion: Geophysical Journal International, **183**, 1401–1407, doi: 10.1111/j.1365-246X.2010.04775.x.

Leggett, J., V. Dubinsky, D. Patterson, and A. Bolshakov, 2001, Field test results demonstrating improved real-time data quality in an advanced LWD acoustic system: SPE, paper 71732.

Pardo, D., P. Matuszyk, I. Muga, C. Torres-Verdín, A. Mora, and V. Calo, 2013, Influence of borehole-eccentered tools in wireline and LWD sonic logging measurements: Geophysical Prospecting, **61**, 268–283, doi: 10.1111/1365-2478.12022.

Rao, R., and M. N. Toksöz, 2005, Dispersive wave analysis — Method and applications: Earth Resources Laboratory Industry Consortia, Annual Report, 2005-04.

Su, Y., X. Tang, S. Xu, and C. Zhuang, 2015, Acoustic isolation of a monopole logging while drilling tool by combining natural stopbands of pipe extensional waves: Geophysical Journal International, **202**, 439–445, doi: 10.1093/gji/ggv150.

Tang, X., D. Patterson, and L. Wu, 2009, Measurement of formation permeability using Stoneley waves from an LWD acoustic tool: Presented at the SPWLA 50th Annual Logging Symposium.

Tao, G., F. He, B. Wang, H. Wang, and P. Chen, 2008, Study on 3D simulation of wave fields in acoustic reflection image logging: Science China: Earth Sciences, **51**, 186–194, doi: 10.1007/s11430-008-6009-6.

Van Kuijk, R., S. Zeroug, B. Froelich, M. Allouche, S. Bose, D. Miller, J. Calvez, and V. Schoepf, 2005, A novel ultrasonic cased-hole imager for enhanced cement evaluation: International Petroleum Technology Conference, paper 10546.

Wang, H., M. Fehler, G. Tao, and Z. Wei, 2016, Investigation of collar properties on data-acquisition scheme for acoustic logging-while-drilling: Geophysics, **81**, no. 6, D611–D624, doi: 10.1190/geo2016-0016.1.

Wang, H., and G. Tao, 2011, Wavefield simulation and data-acquisition-scheme analysis for LWD acoustic tools in very slow formations: Geophysics, **76**, no. 3, E59–E68, doi: 10.1190/1.3552929.

Wang, H., G. Tao, and M. Fehler, 2015, Investigation of the high-frequency wavefield of an off-center monopole acoustic logging-while-drilling tool: Geophysics, **80**, no. 4, D329–D341, doi: 10.1190/geo2014-0426.1.

Wang, H., G. Tao, B. Wang, W. Li, and X. Zhang, 2009b, Wave field simulation and data acquisition scheme analysis for LWD acoustic tool (in Chinese): Chinese Journal of Geophysics, **52**, 2402–2409.

Wang, H., G. Tao, and X. Zhang, 2009a, Review on the development of acoustic logging while drilling (Chinese with English Abstract): Well Logging Technology, **33**, 197–203.

Wang, H., G. Tao, and K. Zhang, 2013a, Wavefield simulation and analysis with the finite-element method for acoustic logging while drilling in horizontal and deviated wells: Geophysics, **78**, no. 6, D525–D543, doi: 10.1190/geo2012-0542.1.

Wang, H., G. Tao, X. Shang, X. Fang, and D. Burns, 2013b, Stability of finite difference numerical simulations of acoustic logging-while-drilling with different perfectly matched layer schemes: Applied Geophysics, **10**, 384–396.